DOI: 10.1021/ic100961w

Inorganic Chemistry
Article

Photophysical Properties and Electropolymerization of Gold Complexes of 3,3″-Diethynyl-2,2′:5′,2″-terthiophene

Angela M. Kuchison, Michael O. Wolf,* and Brian O. Patrick

Department of Chemistry, University of British Columbia, Vancouver, BC, V6T 1Z1, Canada

Received May 13, 2010

The preparation and crystal structures of 3,3″-diethynyl-2,2′:5′,2″-terthiophene (A_2T_3) and three Au(I) complexes containing this ligand are reported. One of the complexes, $Au_2(dppm)(A_2T_3)$, has a short Au−Au distance (3.1969 Å) because of an aurophilic interaction. UV/vis absorption and emission spectra of the complexes and ligand at 298 and 85 K and photoinduced electron transfer to methyl viologen are reported. A_2T_3 and two of the complexes may be electropolymerized, and the resulting gold-containing films were characterized by X-ray photoelectron spectroscopy (XPS) and cyclic voltammetry.

Introduction

Delocalized π electron systems found in conjugated materials impart many interesting properties, including high charge mobility and conductivity, luminescence, and absorption in the UV/vis spectrum to these materials. These properties have led to the use of conjugated materials in applications such as organic photovoltaics,[1] light emitting diodes (OLEDs)[2] and field effect transistors (OFETs).[3,4] Functionalized polythiophenes are some of the most extensively studied conjugated polymers because of their excellent suitability for a variety of electronic applications.[5] Although the extended conjugation found in polythiophenes is important for some of these applications, oligothiophenes with shorter, well-defined conjugation lengths are often useful in evaluating the electronic absorption, emission, and electrochemical properties of related polymers. In some cases the oligomers are also suitable for direct application in electronic devices.[6−11]

Functionalization of oligo- and polythiophenes can be used to achieve an even greater range of materials properties. For example, functionalization with simple alkyl and alkoxy substituents results in greatly enhanced processablity and solubility,[12] while modification with more complex functionalities such as molecular switches,[13] crown ethers[14−16] or fullerenes,[17] results in systems suitable for sensor or molecular electronic (i.e., OFET, photovoltaic or OLED) applications. Metal complexes offer a large range of possible functionality to oligo- and polythiophenes via their optical, catalytic, and electronic properties.[18−21] A particularly intriguing approach to metal modification of conjugated systems is to use the propensity of some metals such as gold to weakly interact with other metal centers, either inter- or intramolecularly. In carefully constructed systems, these "aurophilic" interactions can strongly influence the degree of conjugation in a pendant oligothiophene backbone,[22] and thus dramatically influence the electronic behavior of the oligothiophene. Aurophilic interactions may also give rise to luminescent states which are useful in sensors[23] and

*To whom correspondence should be addressed. E-mail: mwolf@chem.ubc.ca.

(1) Guenes, S.; Neugebauer, H.; Sariciftci, N. S. *Chem. Rev.* **2007**, *107*, 1324–1338.
(2) Mitschke, U.; Bäuerle, P. *J. Mater. Chem.* **2000**, *10*, 1471–1507.
(3) Horowitz, G. *Adv. Mater.* **1998**, *10*, 365–377.
(4) Murphy, A. R.; Frechet, J. M. *J. Chem. Rev.* **2007**, *107*, 1066–1096.
(5) Perepichka, I. F.; Perepichka, D. F. *Handbook of Thiophene-based Materials: Applications in Organic Electronics and Photonics*; John Wiley and Sons, Ltd.: Chichester, West Sussex, U.K., 2009.
(6) Horowitz, G.; Peng, X. Z.; Fichou, D.; Garnier, F. *Synth. Met.* **1992**, *51*, 419–424.
(7) Liu, Y.; Wan, X.; Yin, B.; Zhou, J.; Long, G.; Yin, S.; Chen, Y. *J. Mater. Chem.* **2010**, *20*, 2464–2468.
(8) Wynands, D.; Mannig, B.; Riede, M.; Leo, K.; Brier, E.; Reinold, E.; Bäuerle, P. *J. Appl. Phys.* **2009**, *106*, 054509/1–054509/5.
(9) Thomas, K. R. J.; Hsu, Y. C.; Lin, J. T.; Lee, K. M.; Ho, K. C.; Lai, C. H.; Cheng, Y. M.; Chou, P. T. *Chem. Mater.* **2008**, *20*, 1830–1840.
(10) Barbarella, G.; Favaretto, L.; Zanelli, A.; Gigli, G.; Mazzeo, M.; Anni, M.; Bongini, A. *Adv. Funct. Mater.* **2005**, *15*, 664–670.
(11) Mishra, A.; Ma, C. Q.; Bäuerle, P. *Chem. Rev.* **2009**, *109*, 1141–1276.
(12) Osaka, I.; McCullough, R. D. *Acc. Chem. Res.* **2008**, *41*, 1202–1214.
(13) Finden, J.; Kunz, T. K.; Branda, N. R.; Wolf, M. O. *Adv. Mater.* **2008**, *20*, 1998–2002.
(14) Marsella, M. J.; Swager, T. M. *J. Am. Chem. Soc.* **1993**, *115*, 12214–12215.
(15) Yu, H.-h.; Pullen, A. E.; Bueschel, M. G.; Swager, T. M. *Angew. Chem., Int. Ed.* **2004**, *43*, 3700–3703.
(16) Zhu, S. S.; Swager, T. M. *J. Am. Chem. Soc.* **1997**, *119*, 12568–12577.
(17) Yamazaki, T.; Murata, Y.; Komatsu, K.; Furukawa, K.; Morita, M.; Maruyama, N.; Yamao, T.; Fujita, S. *Org. Lett.* **2004**, *6*, 4865–4868.
(18) Wolf, M. O. *J. Inorg. Organomet.* **2006**, *16*, 189–199.
(19) Moorlag, C.; Sih, B. C.; Stott, T. L.; Wolf, M. O. *J. Mater. Chem.* **2005**, *15*, 2433–2436.
(20) Stott, T. L.; Wolf, M. O. *Coord. Chem. Rev.* **2003**, *246*, 89–101.
(21) Wolf, M. O. *Adv. Mater.* **2001**, *13*, 545–553.
(22) Clot, O.; Akahori, Y.; Moorlag, C.; Leznoff, D. B.; Wolf, M. O.; Batchelor, R. J.; Patrick, B. O.; Ishii, M. *Inorg. Chem.* **2003**, *42*, 2704–2713.
(23) Abdou, H. E.; Mohamed, A. A.; Fackler, J. P.; Burini, A.; Galassi, R.; Lopez-de-Luzuriaga, J. M.; Olmos, M. E. *Coord. Chem. Rev.* **2009**, *253*, 1661–1669.

Published on Web 09/01/2010

Scheme 1. Synthesis of A_2T_3

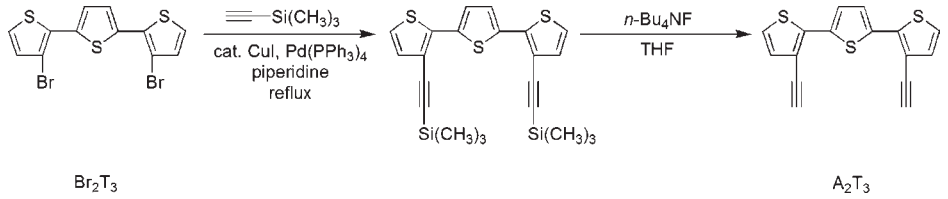

luminescent displays.[24] The presence of aurophilic interactions can therefore affect the electronic properties of Au(I) complexes with oligothiophene ligands, most notably the luminescence that may be either dominated by emission from a Au(I)−Au(I) state or an oligothiophene-based $\pi \leftarrow \pi^*$ state.[25] A variety of ligating groups such as carbenes,[26] thiolates,[27] phosphines,[22,25,28] and acetylides[29,30] have been used to tether Au(I) centers to oligothiophenes.

Oligothiophenes can serve as monomers for the preparation of functionalized polythiophenes,[11] and it is intriguing to consider the possibility of polymerizing oligothiophenes with pendant gold centers that are also involved in aurophilic interactions. This may result in new photophysical behavior and enhanced supramolecular interactions. Previously, we prepared Au complexes where the metal centers were tethered via β-phosphine substituents on adjacent thiophenes, and these species exhibited intramolecular Au−Au interactions.[22] However, the combination of the steric bulk of the diphenylphosphine groups and the poor conjugation between adjacent thiophenes in these complexes prevented electropolymerization.[22] Addition of a third thiophene ring between terminal phosphine-bearing thiophenes resulted in structural changes to the oligothiophene including improved conjugation, but no aurophilic interactions were observed because of the steric bulk of the phosphines.[28] Here we report a new ligand system in which steric effects are reduced via the use of acetylenes rather than diarylphosphines to bind the metals. A terthiophene framework is used to allow planarization of the conjugated backbone. We report three Au(I) complexes with this new ligand, illustrating the effect of aurophilic interactions and ligand conjugation on the photophysical and electrochemical properties of the complexes.

Results and Discussion

Synthesis and Structures. The new diacetylene 3,3″-diethynyl-2,2′:5′,2″-terthiophene (A_2T_3) was prepared from 3,3″-dibromo-2,2′:5′,2″-terthiophene (Br_2T_3).[31] Double Sonagashira coupling of trimethylsilylacetylene to Br_2T_3 gave the trimethylsilyl protected intermediate, which was subsequently deprotected with *n*-Bu_4NF to give A_2T_3 (Scheme 1).

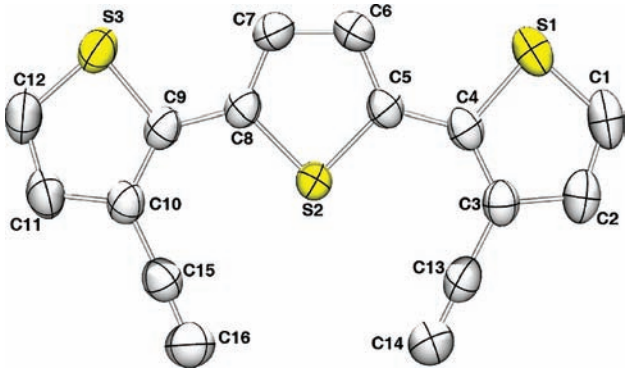

Figure 1. Solid state molecular structure of A_2T_3. Hydrogens have been omitted for clarity and thermal ellipsoids are drawn at 50% probability.

Crystals of A_2T_3 suitable for single crystal X-ray diffraction were grown from a CH_2Cl_2/hexanes solution. In the solid state, the structure of the terthiophene moiety in A_2T_3 (Figure 1) is quite similar to that of unsubstituted 2,2′:5′,2″-terthiophene. A_2T_3 adopts a planar conformation with interannular torsion angles of 4.2 and 8.5°. By comparison, 2,2′:5′,2″-terthiophene has torsion angles ranging from 6° to 9° in the solid state.[32] The terthiophene[32] and acetylene[33] bond lengths and angles are unremarkable, and A_2T_3, like 2,2′:5′,2″-terthiophene,[32] packs in a herringbone structure.

Reaction of A_2T_3 with PPh_3AuCl results in the formation of the digold complex, $(AuPPh_3)_2A_2T_3$ (Scheme 2). Crystals of $(AuPPh_3)_2A_2T_3$ suitable for X-ray diffraction were grown from a $CHCl_3$/hexanes solution, and the solid state molecular structure is shown in Figure 2. The steric bulk imposed by the $AuPPh_3$ group increases the distortion from planarity of the terthienyl backbone (interannular torsion angle: 20.5°) in $(AuPPh_3)_2A_2T_3$ relative to A_2T_3. A related complex in which $AuPPh_3$ centers are coordinated to the terminal (α, α″) positions of a terthiophene was prepared previously.[29] In this case, the metal places less steric demand on the planarity of the terthiophene backbone as evidenced by the small torsion angles of 8.7° and 5.0° in the terthiophene group.[29] Although the Au atoms are on the same side of the A_2T_3 ligand in $(AuPPh_3)_2A_2T_3$, the bulk of the PPh_3 groups prevents an aurophilic interaction.

The PPh_3 ligands in $(AuPPh_3)_2A_2T_3$ can be displaced with less sterically demanding cyanide ligands to give $[n\text{-}Bu_4N]_2[(AuCN)_2A_2T_3]$ (Scheme 2). Crystals of $[n\text{-}Bu_4N]_2[(AuCN)_2A_2T_3]$ were grown from an acetone/diethyl ether solution, and the solid state molecular structure is shown in Figure 3. The bond lengths and angles are

(24) Yam, V. W.-W.; Cheng, E. C.-C. *Top. Curr. Chem.* **2007**, *281*, 269–309.
(25) Stott, T. L.; Wolf, M. O.; Patrick, B. O. *Inorg. Chem.* **2005**, *44*, 620–627.
(26) Powell, A. B.; Bielawski, C. W.; Cowley, A. H. *J. Am. Chem. Soc.* **2009**, *131*, 18232–18233.
(27) Lardiés, N.; Romeo, I.; Cerrada, E.; Laguna, M.; Skabara, P. J. *Dalton Trans.* **2007**, 5329–5338.
(28) Kuchison, A. M.; Wolf, M. O.; Patrick, B. O. *Chem. Commun.* **2009**, 7387–7389.
(29) Li, P.; Ahrens, B.; Choi, K. H.; Khan, M. S.; Raithby, P. R.; Wilson, P. J.; Wong, W. Y. *CrystEngComm* **2002**, *4*, 405–412.
(30) Partyka, D. V.; Gao, L.; Teets, T. S.; Updegraff, J. B.; Deligonul, N.; Gray, T. G. *Organometallics* **2009**, *28*, 6171–6182.
(31) Facchetti, A.; Yoon, M. H.; Stern, C. L.; Hutchison, G. R.; Ratner, M. A.; Marks, T. J. *J. Am. Chem. Soc.* **2004**, *126*, 13480–13501.
(32) Van Bolhuis, F.; Wynberg, H.; Havinga, E. E.; Meijer, E. W.; Staring, E. G. J. *Synth. Met.* **1989**, *30*, 381–389.
(33) Bond, A. D.; Davies, J. E. *Acta Crystallogr., Sect. E: Struct. Rep. Online* **2002**, *E58*, o777–o778.

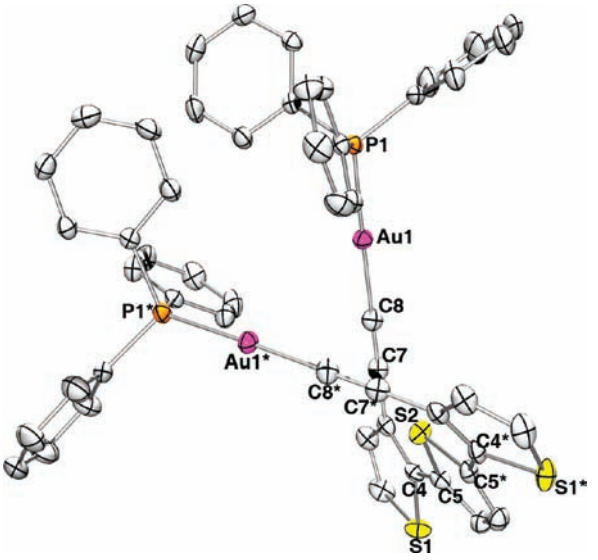

Figure 2. Solid state molecular structure of $(AuPPh_3)_2A_2T_3$. Hydrogens have been omitted for clarity and thermal ellipsoids are drawn at 50% probability.

Scheme 2. Synthesis of $(AuPPh_3)_2A_2T_3$, $[n\text{-}Bu_4N]_2[(AuCN)_2A_2T_3]$ and $Au_2(dppm)(A_2T_3)$

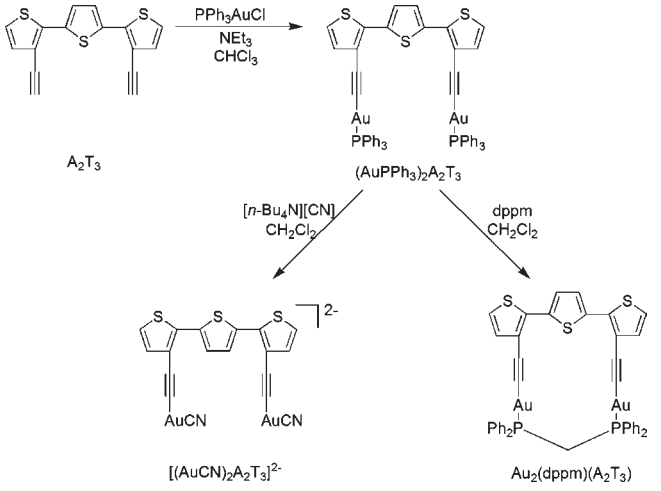

similar to those found in related species.[29,34,35] Despite the decreased steric bulk in $[n\text{-}Bu_4N]_2[(AuCN)_2A_2T_3]$, no aurophilic interactions are observed with the shortest distance between Au centers being 7.5 Å. This is surprising, given that Au(I)−Au(I) interactions are often observed in cationic and anionic Au(I) complexes with low steric bulk around the Au centers.[36] The syn orientation of the thiophene rings in the terthiophene backbone of $[n\text{-}Bu_4N]_2[(AuCN)_2A_2T_3]$ prevents the Au centers from approaching one another. This contrasts with the anti conformation observed in both A_2T_3 and $(AuPPh_3)_2A_2T_3$. In addition, a $[n\text{-}Bu_4N]^+$ counterion is intercalated between adjacent Au atoms in the $[(AuCN)_2A_2T_3]^{2-}$ unit. The planarity of the terthiophene backbone is not significantly altered in the solid state of $[n\text{-}Bu_4N]_2[(AuCN)_2A_2T_3]$ relative to $(AuPPh_3)_2A_2T_3$, as evident from the

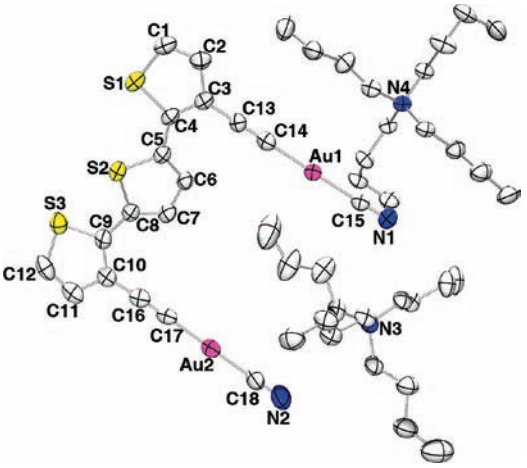

Figure 3. Solid state molecular structure of $[n\text{-}Bu_4N]_2[(AuCN)_2A_2T_3]$. Hydrogens have been omitted for clarity and thermal ellipsoids are drawn at 50% probability.

internannular torsion angles of 19.0° and 20.4° in $[n\text{-}Bu_4N]_2[(AuCN)_2A_2T_3]$.

Reaction of $(AuPPh_3)_2A_2T_3$ with diphenylphosphinomethane (dppm) results in the formation of $Au_2(dppm)(A_2T_3)$. Crystals of this complex were grown from a $CHCl_3-CH_2Cl_2$-acetone solution, and the structure is shown in Figure 4. Here, the dppm bridges the two metal centers, forcing the Au centers into close proximity and resulting in an aurophilic interaction[37] with a Au(1)−Au(2) distance of 3.1969(2)Å. The small bite angle of the dppm forces the Au-acetylide groups to deviate from linearity (C−C−Au = 167.5(3)° and 174.3(4)°). In contrast, $(AuPPh_3)_2A_2T_3$ has a C−C−Au angle of 176.5(3)° and $[n\text{-}Bu_4N]_2[(AuCN)_2A_2T_3]$ has C−C−Au angles of 177.0(3)° and 174.9(4)° (note: C(16B)−C(17B)−Au(2B) is 169(8)°). Of these three Au complexes, $Au_2(dppm)(A_2T_3)$ has the most planar terthiophene backbone with interannular torsion angles of 3.8° and 1.4°. As in $(AuPPh_3)_2A_2T_3$, all of the S atoms in $Au_2(dppm)(A_2T_3)$ are anti to each other. In this case, this conformation minimizes the distance between Au centers and allows the Au−Au interaction in $Au_2(dppm)(A_2T_3)$. In contrast, other phosphino-Au-thienyl complexes with intramolecular aurophilic interactions have torsion angles of ~100° between adjacent rings and Au−Au distances of 3.0879(7) and 3.3322(4) Å.[22]

Electronic Spectroscopy

UV/vis Absorption Spectra. The UV/vis absorption spectra of A_2T_3, $(AuPPh)_3A_2T_3$, $[n\text{-}Bu_4N]_2[(AuCN)_2A_2T_3]$, and $Au_2(dppm)(A_2T_3)$ are shown in Figure 5. The spectra are dominated by strong $\pi\rightarrow\pi^*$ transitions. The spectrum of A_2T_3 has two absorption bands (Table 1) slightly red-shifted from the corresponding bands in the spectrum of 2,2′:5′,2″-terthiophene (λ_{max} = 250 and 354 nm)[38] since unsubstituted terthiophene does not benefit from the additional conjugation afforded by the acetylene groups. Coordination of the Au centers to the acetylene results in small shifts of the highest energy

(34) Katz, M. J.; Leznoff, D. B. *J. Am. Chem. Soc.* **2009**, *131*, 18435–18444.
(35) Rosenzweig, A.; Cromer, D. T. *Acta Crystallogr.* **1959**, *12*, 709–712.
(36) Balch, A. L. *Struct. Bonding* (*Berlin*) **2007**, *123*, 1–40.
(37) Bardaji, M.; Laguna, A. *J. Chem. Educ.* **1999**, *76*, 201–203.
(38) Becker, R. S.; de Melo, J. S.; Maçanita, A. L.; Elisei, F. *J. Phys. Chem.* **1996**, *100*, 18683–18695.

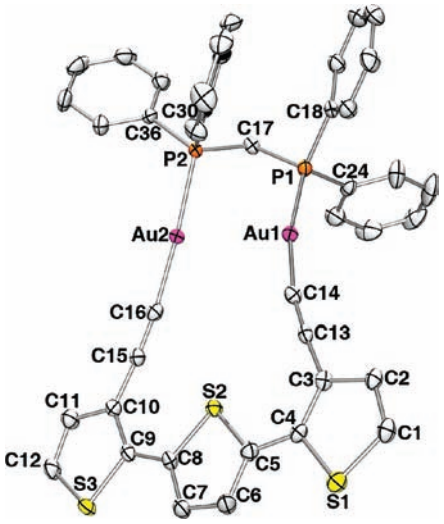

Figure 4. Solid state molecular structure of $Au_2(dppm)(A_2T_3)$. Hydrogens and occluded solvent have been omitted for clarity and thermal ellipsoids are drawn at 50% probability.

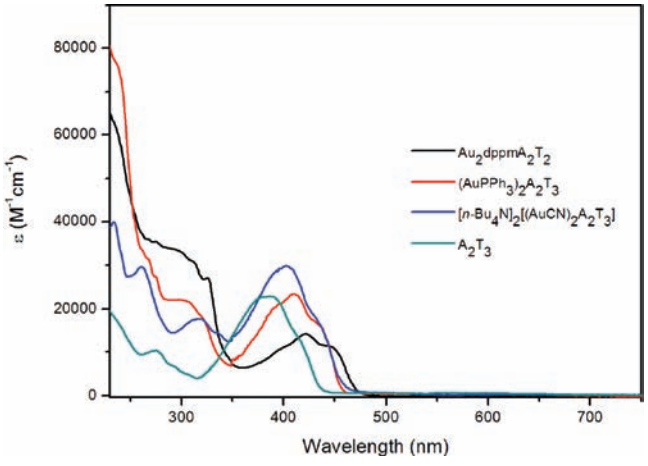

Figure 5. UV/vis absorption spectra of A_2T_3, $(AuPPh_3)_2A_2T_3$, $[n\text{-}Bu_4N]_2[(AuCN)_2A_2T_3]$, and $Au_2(dppm)(A_2T_3)$ in CH_2Cl_2 at 298 K.

$\pi \rightarrow \pi^*$ transition, as has been previously observed for other Au(I)-acetylide complexes,[39] and is most clearly evident in $[n\text{-}Bu_4N]_2[(AuCN)_2A_2T_3]$ where $\lambda_{max} = 260$ nm. In $(AuPPh_3)_2A_2T_3$ and $Au_2(dppm)(A_2T_3)$, the higher energy transitions consist of a combination of the $\pi \rightarrow \pi^*$ transitions of the phenyl rings of PPh_3 and dppm as well as A_2T_3 based $\pi \rightarrow \pi^*$ transitions. The lower energy bands in the gold complexes are all red-shifted with respect to the lower energy band in A_2T_3, as previously observed in related complexes.[29] The red-shift has previously been attributed to electronic interactions of the acetylide ligand with $AuPPh_3$, and was found to depend on whether one or two $AuPPh_3$ groups are coordinated.[29] By contrast, the compounds discussed here demonstrate that changing the peripheral ligands on the $Au_2A_2T_3$ moiety changes the electronic interaction of the Au with the A_2T_3. The larger red-shift of the lowest energy transition of $Au_2(dppm)(A_2T_3)$ is not only an electronic effect due to the presence of the dppm ligand but also a result of the increased conjugation along the terthiophene backbone imposed by the molecular geometry. Additional bands between 300 and 330 nm in the spectra of $Au_2(dppm)(A_2T_3)$, $(AuPPh_3)_2A_2T_3$, and $[n\text{-}Bu_4N]_2[(AuCN)_2A_2T_3]$ may be due to metal-perturbed intraligand transitions. Several other gold acetylide complexes have bands with contributions of a similar nature.[39−42]

Low temperature UV/vis spectra of the molecules in MeOH/EtOH glasses were obtained to gain further insight into their electronic behavior. In an EtOH/MeOH (4:1) solution at room temperature, the absorption spectra of all the compounds are similar to those obtained in CH_2Cl_2. In a frozen MeOH/EtOH glass at 85 K, increased vibronic coupling is observed for all the compounds (Figure 6). The lowest energy electronic transition for all the compounds, observed as a single broad band at room temperature, separates into several bands at 85 K with $\sim$1400−1490 cm^{-1} spacing. This vibronic coupling is attributed to thiophene ring vibrations[43] and C−C stretches.[44] Low temperature studies on 2,2′:5′,2″-terthiophene show similar vibronic structure.[38,45] In the case of A_2T_3 and $[n\text{-}Bu_4N]_2[(AuCN)_2A_2T_3]$ there appear to be additional sharp bands in the lower energy region of the spectrum. These may be due to C−H vibronic coupling or the presence of multiple structural conformations frozen out at low temperature. The higher energy transitions also show vibronic coupling with the thienyl rings, consistent with an electronically delocalized system.

The spectra of all the compounds exhibit a bathochromic shift in the lowest energy band with decreasing temperature. For A_2T_3, the absorption red-shifts by $\sim$900 cm^{-1} upon cooling to 85 K. The absorption band of 2,2′:5′,2″-terthiophene is known to bathochromically shift by $\sim$1600 cm^{-1} from room temperature to 77 K.[38] This has been attributed to increased planarity of the terthienyl group at low temperature resulting in increased conjugation, and a similar effect is likely involved here. At low temperature, the spectra of the Au(I) complexes are considerably less red-shifted than the spectrum of A_2T_3. At 85 K the lowest energy absorption bands are bathochromically shifted by $\sim$480 cm^{-1}, $\sim$450 cm^{-1}, and $\sim$360 cm^{-1} for $[n\text{-}Bu_4N]_2[(AuCN)_2A_2T_3]$, $Au_2(dppm)(A_2T_3)$, and $(AuPPh_3)_2A_2T_3$, respectively. This suggests that the presence of the Au(I) centers restrict rotation of the thienyl units more than in free A_2T_3 which is not hindered by the metal centers.

Emission Spectra. A_2T_3, $(AuPPh_3)_2A_2T_3$, and $[n\text{-}Bu_4N]_2[(AuCN)_2A_2T_3]$ are all emissive at room temperature. The excitation and emission spectra of these compounds in CH_2Cl_2 solution are shown in Figure 7. The excitation spectra of the molecules match their respective electronic absorption spectra, except <300 nm where the low intensity

(39) Yam, V. W.-W.; Choi, S. W.-K. *J. Chem. Soc., Dalton Trans.* **1996**, 4227–4232.

(40) Yam, V. W. W.; Lo, K. K. W.; Wong, K. M. C. *J. Organomet. Chem.* **1999**, *578*, 3–30.

(41) Bardaji, M.; Jones, P. G.; Laguna, A. *J. Chem. Soc., Dalton Trans.* **2002**, 3624–3629.

(42) Li, D.; Hong, X.; Che, C. M.; Lo, W. C.; Peng, S. M. *J. Chem. Soc., Dalton Trans.* **1993**, 2929–2932.

(43) Tsukerman, S. V.; Nikitchenko, V. M.; Rozum, Y. S.; Lavrushin, V. F. *Khim. Geterotsikl. Soedin.* (*Engl. Transl.*) **1967**, 452–458.

(44) Svedberg, F.; Alaverdyan, Y.; Johansson, P.; Kaell, M. *J. Phys. Chem. B* **2006**, *110*, 25671–25677.

(45) DiCésare, N.; Belletête, M.; Marrano, C.; Leclerc, M.; Durocher, G. *J. Phys. Chem. A* **1999**, *103*, 795–802.

Table 1. Absorption Data for Compounds at 298 K in CH_2Cl_2 Solutions and 85 K in MeOH/EtOH

compound	λ_{max} /nm (ε_{max}/M^{-1} cm^{-1}) at 298 K	λ_{max}/nm at 85 K
A_2T_3	274 (9 000), 385 (21 000)	271 (sh), 280, 295, 308, 379, 393 (sh), 401, 419 (sh), 427
$(AuPPh_3)_2A_2T_3$	267 (34 000), 307 (24 000), 411 (24 000)	262, 303, 323 (sh), 390, 412, 438
$[n\text{-}Bu_4N]_2[(AuCN)_2A_2T_3]$	260 (25 000), 320 (18 000), 404 (25 000)	259, 310, 322, 393, 409, 414, 435, 441 (sh)
$Au_2(dppm)(A_2T_3)$	301 (33 000), 326 (28 000), 421 (15 000)	268, 275, 289, 312, 326, 400, 425, 454

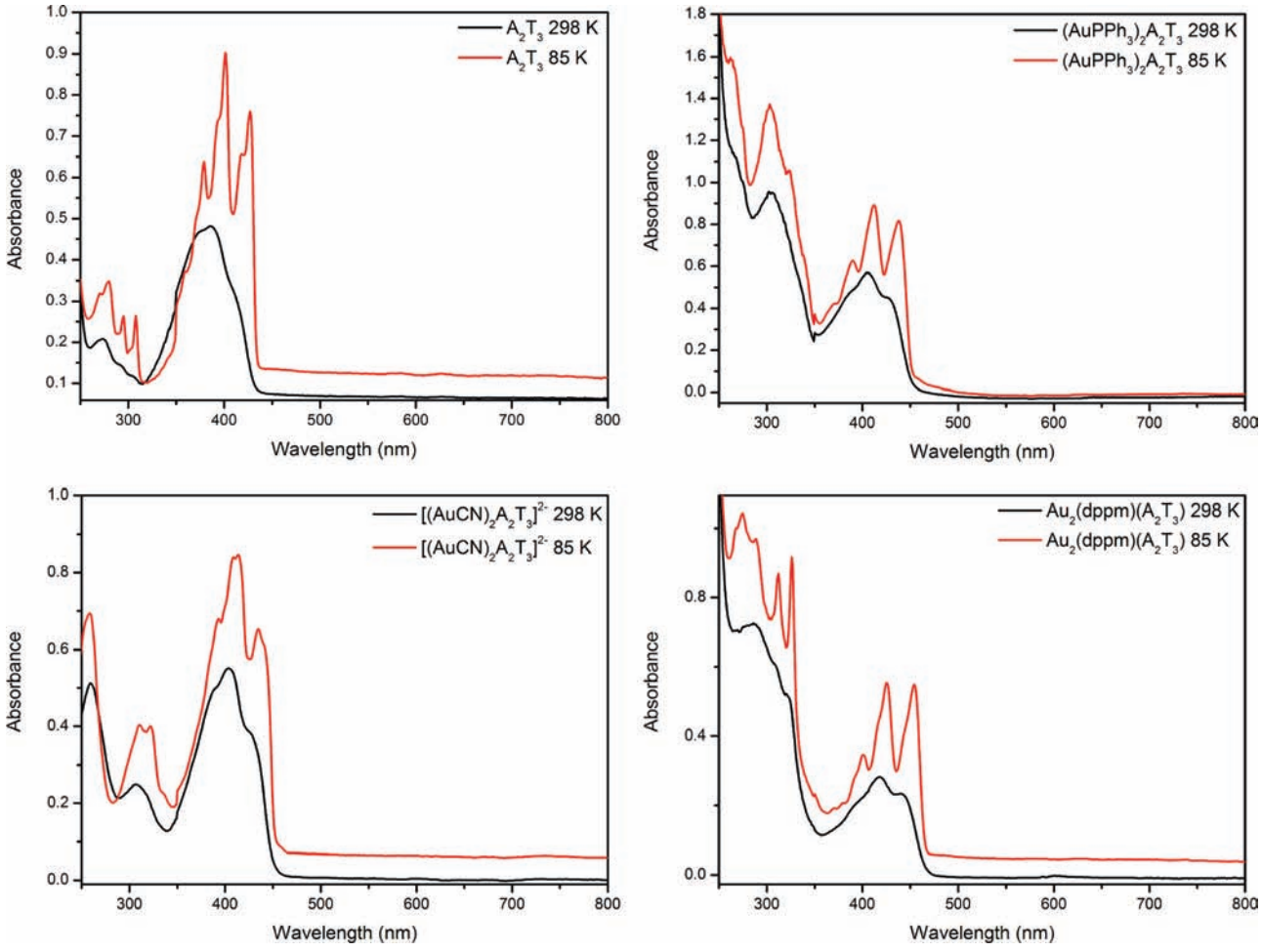

Figure 6. Comparison of 298 and 85 K absorption spectra of A_2T_3, $(AuPPh_3)_2A_2T_3$, $[n\text{-}Bu_4N]_2[(AuCN)_2A_2T_3]$, and $Au_2(dppm)(A_2T_3)$ in MeOH/EtOH.

of the xenon lamp results in weak emission. The emission spectrum of A_2T_3 is similar to that of 5,5″-bis(acetylene)-terthiophene (λ_{em} = 446 and 469 nm)[29] and 2,2′:5′,2″-terthiophene (λ_{em} = 407 and 426 nm),[38] with ring vibrations coupled in all three cases. The emission bands of $(AuPPh_3)_2A_2T_3$ and $[n\text{-}Bu_4N]_2[(AuCN)_2A_2T_3]$ are red-shifted with respect to those of A_2T_3 (Figure 6, Table 2). All of the compounds which are emissive at room temperature had excited state lifetimes of < 50 ps. Such short lifetimes are typical of fluorescence of terthiophene derivatives. For example, emission lifetimes of phosphonic acid monoethyl ester and carboxylic acid derivatized terthiophenes are ~20 and 200 ps, respectively.[46,47] Emission quantum yields (Φ_{em}) were measured where possible (Table 2), and are generally low; however, the Au complexes both have a smaller quantum yield than A_2T_3 possibly a result of the heavy-atom effect.[48] The small Stokes shift, similar band shape of the emission to that of A_2T_3, and short emission lifetimes of the Au complexes are consistent with ligand-based emission from a singlet state.

Unlike the other compounds, $Au_2(dppm)(A_2T_3)$ is non-emissive at room temperature. This suggests that either radiationless decay dominates the relaxation of the excited state or any emission is too weak to be observed. There are several Au(I) complexes known where ligand phosphorescence is the dominant emission observed in solution,[42,49,50] and it is possible that this also occurs in $Au_2(dppm)(A_2T_3)$. Since the terthienyl group in $Au_2(dppm)(A_2T_3)$ is remarkably planar, the ligand-based

(46) Beek, W. J. E.; Janssen, R. A. J. *J. Mater. Chem.* **2004**, *14*, 2795–2800.
(47) Anestopoulos, D.; Fakis, M.; Mousdis, G.; Giannetas, V.; Persephonis, P. *Synth. Met.* **2007**, *157*, 30–34.
(48) Berberan-Santos, M. N. *PhysChemComm* **2000**, *3*, 18–23.
(49) Osawa, M.; Hoshino, M.; Akita, M.; Wada, T. *Inorg. Chem.* **2005**, *44*, 1157–1159.
(50) Fernández, E. J.; Laguna, A.; López-de-Luzuriaga, J. M.; Monge, M.; Montiel, M.; Olmos, M. E.; Rodríguez-Castillo, M. *Dalton Trans.* **2006**, 3672–3677.

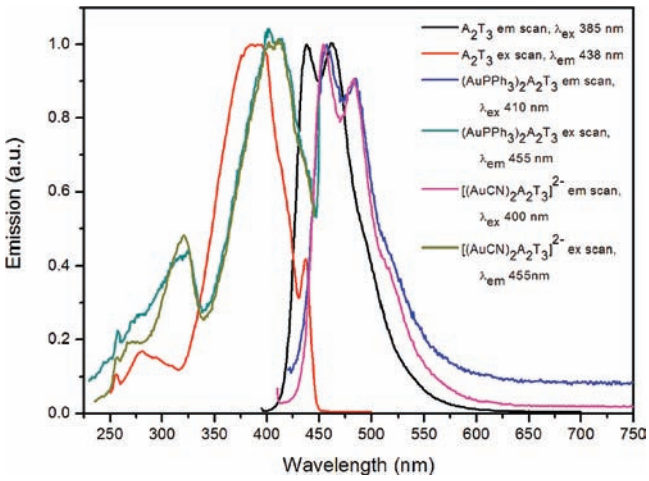

Figure 7. Emission and Excitation Spectra of A_2T_3, $(AuPPh_3)_2A_2T_3$, and $[n\text{-}Bu_4N]_2[(AuCN)_2A_2T_3]$ in CH_2Cl_2 at 298 K.

Table 2. Emission Data for Compounds at 298 K in CH_2Cl_2 and 85 K in MeOH/EtOH

compound	λ_{em}/nm at 298 K	λ_{em}/nm at 85 K	Φ_{em} (298 K)
A_2T_3	438, 462	432, 461, 493, 529	0.042
$(AuPPh_3)_2A_2T_3$	452, 479	451, 482, 517, 559	0.016
$[n\text{-}Bu_4N]_2[(AuCN)_2A_2T_3]$	447, 475	448, 478, 511, 553	0.032
$Au_2(dppm)(A_2T_3)$		465, 498, 536, 581	

triplet state may be populated more readily than in $[n\text{-}Bu_4N]_2[(AuCN)_2A_2T_3]$ or $(AuPPh_3)_2A_2T_3$. Sparging a solution of $Au_2(dppm)(A_2T_3)$ with nitrogen gas did not result in any observable emission. Phosphorescence from 2,2′:5′,2″-terthiophene is difficult to observe, but has been reported at 826 nm at 18 K[51] and at 682 nm at 80 K using nanosecond excitation with gated detection.[52] Such experimental difficulties may complicate the observation of a thiophene-based triplet emission from $Au_2(dppm)(A_2T_3)$. Alternatively, radiationless decay because of Au(I)−Au(I) states may occur. Gold-based emission is sensitive to the ligands present and these can result in non-emissive interactions.[53]

Interestingly, $Au_2(dppm)(A_2T_3)$ is emissive at low temperature. The emission bands are red-shifted with respect to those seen in the other compounds (Table 2). As in $(AuPPh_3)_2A_2T_3$ and $[n\text{-}Bu_4N]_2[(AuCN)_2A_2T_3]$, the small Stokes shift between the excitation and emission bands of $Au_2(dppm)(A_2T_3)$ is consistent with ligand-based emission. The strong emission from $Au_2(dppm)(A_2T_3)$ at 85 K decreases with increasing temperature and is essentially gone >185 K (Figure 8).

As observed in the absorption spectra, the low temperature emission spectra show vibronic coupling with the thiophene ring vibrations (Figure 8 and 9). The 85 K emission spectra for A_2T_3, $(AuPPh_3)_2A_2T_3$, $[n\text{-}Bu_4N]_2[(AuCN)_2A_2T_3]$, and $Au_2(dppm)(A_2T_3)$ all have four bands separated by $\sim$1400 cm^{-1}. The low energy region of the excitation spectra match the respective absorption

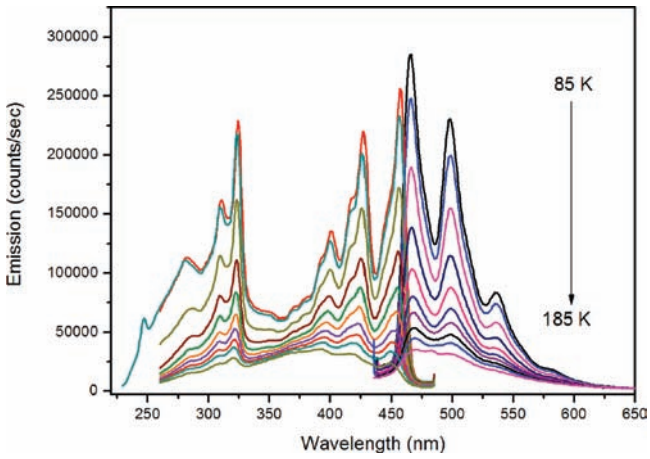

Figure 8. Emission (right side) and excitation (left side) spectra of $Au_2(dppm)(A_2T_3)$ as a function of temperature in MeOH/EtOH.

spectra at low temperature in all cases. Unlike the absorption spectra, the emission bands do not shift with decreasing temperature. This indicates that fluorescence is likely occurring from a state localized on the planar oligothiophene backbone as has previously been observed in 2,2′:5′,2″-terthiophene.[38] The intensity of the emission also increased with decreasing temperature, consistent with reduced nonradiative decay pathways at low temperature.

Photoinduced Electron Transfer. It has previously been shown in separate studies that terthiophene derivatives,[54,55] bis-Au(I) complexes,[56] and Au(I) acetylide complexes[39,42] are capable of undergoing photoinduced electron transfer (PET) to methyl viologen (MV^{2+}). The presence of several of these same structural features in the complexes discussed here suggested the possibility of photoinduced electron transfer occurring in these complexes. This type of excited state reactivity is of interest for potential applications in solar energy harvesting and hydrogen photogeneration.[57]

The excited state oxidation potentials ($E(M/M^+)^*$) of $(AuPPh_3)_2A_2T_3$, $[n\text{-}Bu_4N]_2[(AuCN)_2A_2T_3]$, $Au_2(dppm)(A_2T_3)$, and A_2T_3 were calculated using eq 1 where $E(M/M^+)$ is the first electrochemical oxidation potential and E^* is emission energy.[58] The calculated singlet excited state redox potentials are shown in Table 3.

$$E(M/M^+)^* = E(M/M^+) - E^* \quad (1)$$

Given that the reduction potential of $(MV^{2+}/MV^{+\cdot})$ is -0.69 V versus SCE,[59] it is predicted that the singlet states of A_2T_3 and all of the gold complexes are thermodynamically capable of photoreducing MV^{2+}.

Irradiation of CH_3CN solutions of A_2T_3 and MV^{2+} with white or UV light results in a substantial decrease in

(51) Xu, B.; Holdcroft, S. *J. Am. Chem. Soc.* **1993**, *115*, 8447–8448.
(52) Wasserberg, D.; Marsal, P.; Meskers, S. C. J.; Janssen, R. A. J.; Beljonne, D. *J. Phys. Chem. B* **2005**, *109*, 4410–4415.
(53) Tiekink, E. R. T.; Kang, J. G. *Coord. Chem. Rev.* **2009**, *253*, 1627–1648.
(54) Kim, Y. S.; McNiven, S.; Ikebukuro, K.; Karube, I. *Photochem. Photobiol.* **1997**, *66*, 180–184.
(55) Evans, C. H.; Scaiano, J. C. *J. Am. Chem. Soc.* **1990**, *112*, 2694–2701.
(56) Che, C. M.; Kwong, H. L.; Yam, V. W. W.; Cho, K. C. *J. Chem. Soc., Chem. Commun.* **1989**, 885–886.
(57) Kalyanasundaram, K. *Coord. Chem. Rev.* **1982**, *46*, 159–244.
(58) Kalyanasundaram, K. *Photochemistry of Polypyridine and Porphyrin Complexes*; Academic Press Limited: Toronto, 1992.
(59) Peon, J.; Tan, X.; Hoerner, J. D.; Xia, C.; Luk, Y. F.; Kohler, B. *J. Phys. Chem. A* **2001**, *105*, 5768–5777.

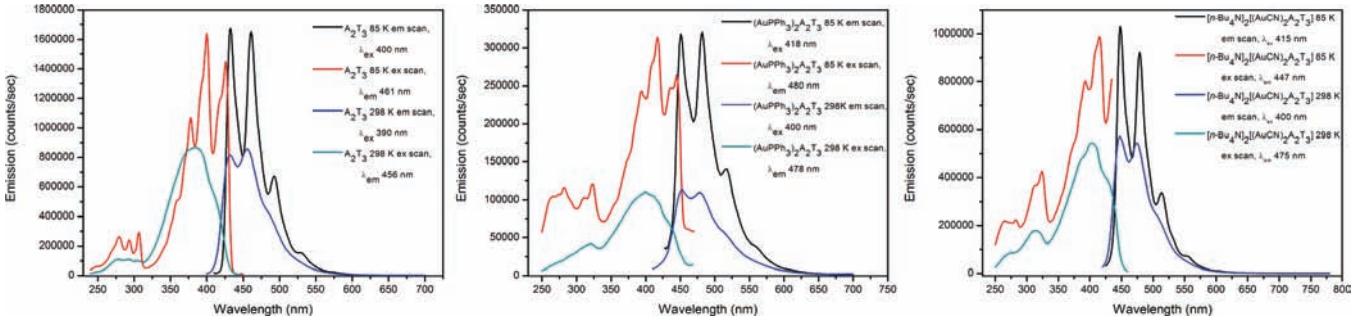

Figure 9. Comparison of room temperature excitation and emission spectra of A_2T_3, $(AuPPh_3)_2A_2T_3$, and $[n\text{-}Bu_4N]_2[(AuCN)_2A_2T_3]$ in EtOH−MeOH.

Table 3. Calculated Singlet Excited State Redox Potentials of Compounds

compound	$E(M/M^+)^*$ (V vs SCE)
A_2T_3	−1.77
$(AuPPh_3)_2A_2T_3$	−1.40
$[n\text{-}Bu_4N]_2[(AuCN)_2A_2T_3]$	−1.84
$Au_2(dppm)(A_2T_3)$	−1.90

the intensity of the A_2T_3 absorption band at 385 nm (Supporting Information, Figure S1 and S2). The characteristic blue color of the $MV^{+\cdot}$ radical cation was not observed after this irradiation. Irradiation of A_2T_3 in the absence of MV^{2+} under the same conditions did not result in a decrease in the absorption band intensity. These results suggest some interaction between A_2T_3 and MV^{2+} occurs upon irradiation, possibly resulting in decomposition of the A_2T_3; however, there is no evidence for PET.

None of the gold compounds show significant decomposition with light irradiation in CH_3CN. A shoulder appears at 470 nm in the absorbance spectrum of $[n\text{-}Bu_4N]_2[(AuCN)_2A_2T_3]$ when left in solution overnight. Since this suggests possible thermal decomposition, solutions of $[n\text{-}Bu_4N]_2[(AuCN)_2A_2T_3]$ were used immediately after preparation. The spectra of $(AuPPh_3)_2A_2T_3$ or $Au_2(dppm)(A_2T_3)$ remained stable when solutions were left overnight.

Irradiation of $(AuPPh_3)_2A_2T_3/MV^{2+}$ solutions with either UV or white light resulted in the appearance of absorption bands due to $MV^{+\cdot}$ (Supporting Information, Figure S3 and S4).[60] The short emission lifetime for this complex suggests that either intermolecular electron transfer from the singlet state is extremely rapid, or another, non-emissive, excited state is involved in the electron transfer.

Despite excited $[n\text{-}Bu_4N]_2[(AuCN)_2A_2T_3]$ being thermodynamically a stronger reducing agent than $(AuPPh_3)_2A_2T_3$, UV and white light irradiation resulted in no absorption due to $MV^{+\cdot}$. It is possible that there is a large activation barrier for electron transfer, or that $[(AuCN)_2A_2T_3]^{2-}$ and MV^{2+} form an ion-pair in solution causing back-electron transfer to be rapid. $[Au(CN)_2]^-$ has been prepared with a MV^{2+} counterion;[61] however, there are no literature reports of electron transfer from $[Au(CN)_2]^-$ to MV^{2+} to yield $MV^{+\cdot}$.

Interestingly, substituting PPh_3 for dppm results in different excited state properties. Photoexcitation of a CH_3CN solution of $Au_2(dppm)(A_2T_3)/MV^{2+}$ solution

Scheme 3

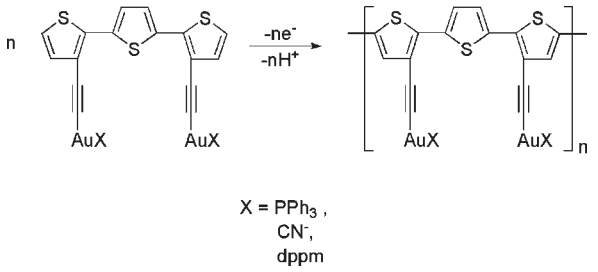

with UV light resulted in the observation of $MV^{+\cdot}$, but white light did not. This suggests that population of the higher energy states is required for electron transfer. These differences may be related to either the rigidity or the aurophilic interaction of $Au_2(dppm)(A_2T_3)$.

Electropolymerization. Oligothiophene complexes may be electropolymerized, giving materials with longer conjugation lengths. Previously, Lardiés et al.[27] and Powell et al.[26] have electropolymerized Au(I)-thienyl complexes. The presence of aurophilic interactions in digold-phosphine complexes resulted in substantial interannular twisting of the oligothiophene backbone which prevents electropolymerization.[22] $(AuPPh_3)_2A_2T_3$, $[n\text{-}Bu_4N]_2[(AuCN)_2A_2T_3]$, and $Au_2(dppm)(A_2T_3)$ have relatively planar terthiophene ligands and thus are good candidates for electropolymerization. The oxidative electropolymerization reaction of the Au complexes, and the proposed structure of the products are shown in Scheme 3.

The cyclic voltammogram (CV) of A_2T_3 has one oxidation wave at 1.00 V versus SCE that increases in current with increasing number of scans (Supporting Information, Figure S6). This behavior is characteristic of the electropolymerization of a conductive polymer on the working electrode. Both acetylene and thiophene are known to electropolymerize and have similar oxidation potentials,[62,63] so it is difficult to predict the structure of the electropolymerized A_2T_3.

Cyclic voltammetry of $(AuPPh_3)A_2T_3$ shows one irreversible oxidation wave at 1.16 V versus SCE. Repeated scans resulted in increased current with each subsequent oxidation wave (Figure 10a), thus showing evidence that electropolymerization is occurring. As the number of scans is increased, the oxidation wave also shifted to

(60) Kosower, E. M.; Cotter, J. L. *J. Am. Chem. Soc.* **1964**, *86*, 5524–5527.
(61) Kunkely, H.; Vogler, A. *Inorg. Chem. Commun.* **2000**, *3*, 205–207.
(62) García-Cañadas, J.; Rodríguez, J. G.; Lafuente, A.; Marcos, M. L.; Velasco, J. G. *J. Polym. Sci., Part A: Polym. Chem.* **2005**, *43*, 2407–2416.
(63) Roncali, J.; Garreau, R.; Yassar, A.; Marque, P.; Gamier, F.; Lemaire, M. *J. Phys. Chem.* **1987**, *91*, 6706–6714.

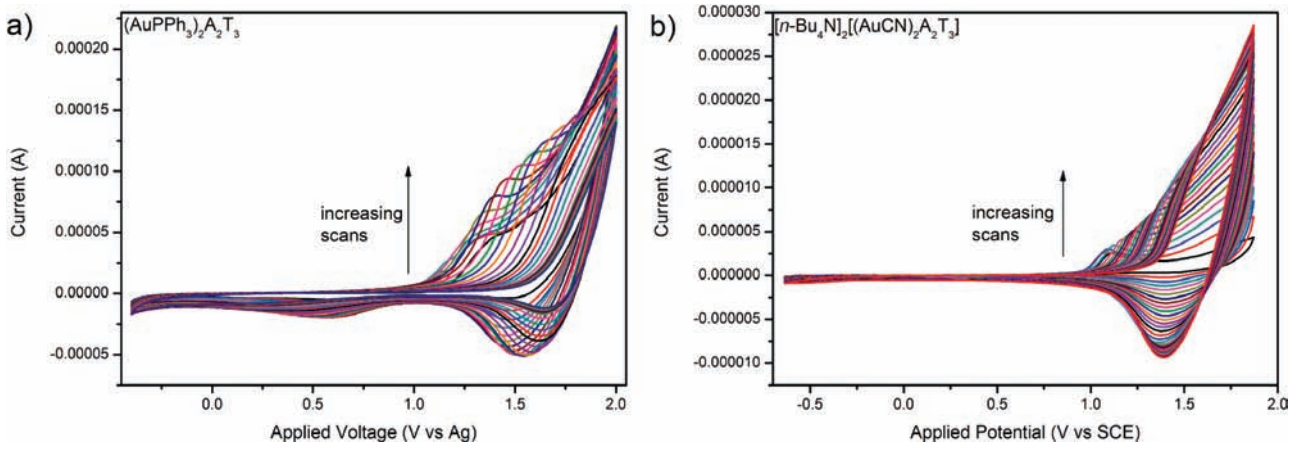

Figure 10. Electropolymerization of (a) $(AuPPh_3)_2A_2T_3$ on an ITO electrode and (b) electropolymerization of $[n\text{-}Bu_4N]_2[(AuCN)_2A_2T_3]$ on a Pt disk electrode. Scan rate = 100 mV/s. Solvent = CH_2Cl_2. Electrolyte = 0.1 M $[n\text{-}Bu_4N][PF_6]$.

Table 4. XPS Analysis Data of Electropolymerized Films

compound	sample no.	%Au	%S	%P	%N	Au:S	Au:N	Au:P
poly-$(AuPPh_3)_2A_2T_3$	1	0.27	8.50			1:31		
	2	0.51	8.72	0.98		1:17		1:1.9
	3	0.44	9.68	0.59		1:22		1:1.3
poly-$[n\text{-}Bu_4N]_2[(AuCN)_2A_2T_3]$	1	5.50	10.07		3.79	1:1.8	1:0.6	
poly-$Au_2(dppm)(A_2T_3)$	1	1.75	6.87	2.67		1:3.9		1:1.5
	2	2.18	5.81	3.13		1:2.6		1:1.4
	3	0.77	6.23	0.61		1:8.1		1:0.8

higher potential. This shift suggests that either the conjugation in the electropolymerized material is less than in the monomer, or that a poorly conductive material forms as a consequence of the electropolymerization. With two large $AuPPh_3$ groups close together, steric interactions may cause twisting along the oligo/polythiophene backbone. Lardiés et al. also observed an increase in oxidation potential with increasing scans during electropolymerization.[27] X-ray photoelectron spectroscopy (XPS) analysis of the films prepared here revealed a lower Au content than would be expected from the monomer formula, despite analytically pure monomer being used (Table 4). Metal-acetylide bonds are stablilized by ionic character,[64] and it is possible that oxidative electropolymerization decreases the Au−C bond strength allowing $[AuPPh_3]^+$ to dissociate from the polymer. A reduction wave is observed at 0.5 V. Waves at similar potentials are observed for Au nanoparticles and are attributed to reduction of Au oxide.[65] It is possible that Au(0) particles are formed by loss and reduction of Au from the polymer. Alternatively, this could indicate poly-A_2T_3 formation since a similar reduction wave is observed during electropolymerization of A_2T_3 (Supporting Information, Figure S6). The presence of this wave with repetitive scanning may indicate loss of Au from the polymer is occurring.

The complex $[n\text{-}Bu_4N]_2[(AuCN)_2A_2T_3]$ also has one irreversible oxidation wave at 1.08 V versus SCE (Figure 10b). With increasing scans, the oxidation wave became quasireversible, and the current increases, as expected for electropolymerization on the working electrode surface. XPS data shows the same Au/S elemental composition as the $[n\text{-}Bu_4N]_2[(AuCN)_2A_2T_3]$ monomer supporting the conclusion that the Au-acetylide complex remains intact. The lower nitrogen content suggests less counterion may be present in the polymer than in the monomer and could indicate some p-doping of the resulting polythiophene. Doped polymer would carry a positive charge on the backbone balancing the negative charge at the metal, thus no longer requiring counterions for charge balance.

Similarly, the growth in the oxidation wave of an $Au_2(dppm)(A_2T_3)$ solution with increasing scans indicates electropolymerization of this complex (Figure 11a). The CV of $Au_2(dppm)(A_2T_3)$ has two oxidation waves, one at 0.76 V and another at 1.51 V versus SCE. Metal−metal interactions are known to stabilize Au^{2+} centers.[66] For example, $[(Au_2\{\mu\text{-}(CH_2)_2PPh_2\}(\mu\text{-dppa})][ClO_4]$ (dppa = $Ph_2PNHPPh_2$) has an irreversible oxidation wave at 0.92 V[67] while $[Au_2(\mu\text{-}CH_2PPh_2CH_2)_2]$ oxidizes at 0.11 V.[68] Repetitive scanning past the first oxidation wave of $Au_2(dppm)(A_2T_3)$ resulted in no increase in current, which suggests the oxidation wave at 0.76 V is from a $Au^{+/2+}$ oxidation process. Scanning to higher potential resulted in increased conductivity and therefore polymer formation, which suggests the oxidation wave at 1.51 V is from a terthiophene-based oxidation. A reduction wave, similar to that found in the CV of $(AuPPh_3)_2A_2T_3$, appears at −0.35 V and increases with repetitive scans. Repetitive scans resulted in a shiny yellow-gold film on the working electrode. The XPS analysis on the poly-$Au_2(dppm)(A_2T_3)$ film indicates slightly less Au than expected from

(64) Kaharu, T.; Ishii, R.; Adachi, T.; Yoshida, T.; Takahashi, S. *J. Mater. Chem.* **1995**, *5*, 687–692.
(65) Kumar, S.; Zou, S. *Langmuir* **2009**, *25*, 574–581.
(66) Laguna, A.; Laguna, M. *Coord. Chem. Rev.* **1999**, *193*−*195*, 837–856.
(67) Bardaji, M.; Connelly, N. G.; Gimeno, M. C.; Jimenez, J.; Jones, P. G.; Laguna, A.; Laguna, M. *J. Chem. Soc., Dalton Trans.* **1994**, 1163–1167.
(68) Bardaji, M.; Jones, P. G.; Laguna, A.; Laguna, M. *Organometallics* **1995**, *14*, 1310–1315.

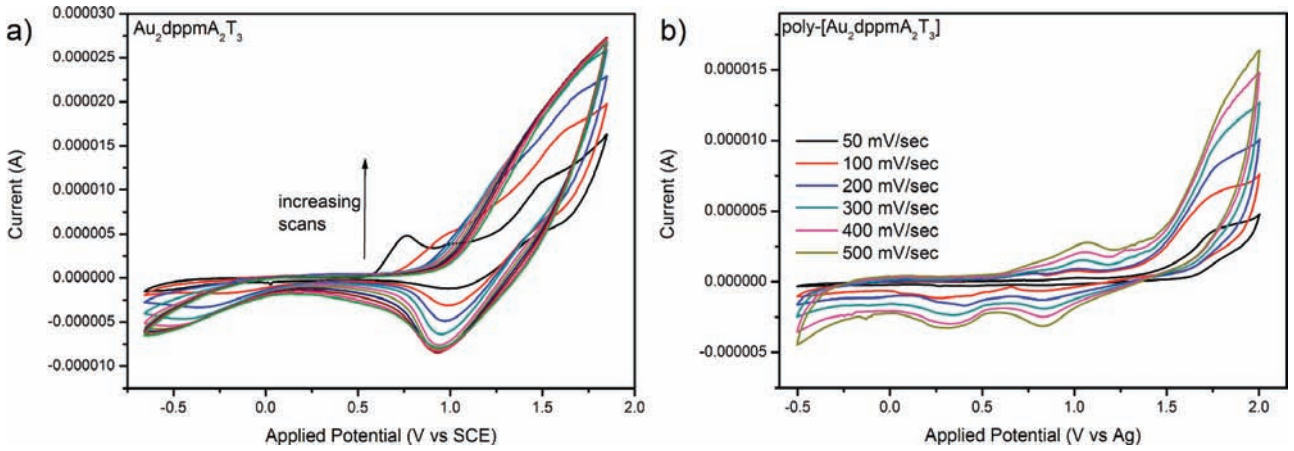

Figure 11. (a) Electropolymerization of $Au_2(dppm)(A_2T_3)$ on a Pt disk electrode (Scan rate = 100 mV/s) and (b) CV of poly-$Au_2(dppm)(A_2T_3)$ at a Pt disk electrode in monomer-free solution. Electrolyte = 0.1 M [*n*-Bu_4N][PF_6]. Solvent = CH_2Cl_2.

the monomer formula is present, but does not show the same dramatic loss of Au as in poly-$(AuPPh_3)_2A_2T_3$. The bridging dppm and the lower steric bulk of this ligand relative to PPh_3 may inhibit $[Au_2dppm]^{2+}$ dissociation during electropolymerization. Interestingly, a poly-$Au_2(dppm)(A_2T_3)$ film in monomer free solution showed a $Au^{+/2+}$ oxidation wave in addition to the polythiophene oxidation wave as shown in Figure 11b which suggests that the Au−Au interaction persists in the polymerized material.

Conclusions

The new conjugated diacetylene A_2T_3 and the three gold complexes containing this ligand reported here reveal some interesting aspects of the electronic properties of metal-containing oligothiophenes. Two structural aspects of the gold complexes: the presence or absence of aurophilic interactions and the conjugation in the oligothiophene backbone, are relevant in understanding the electronic behavior of the complexes. It is apparent that steric constraints prevent aurophilic interactions from occurring in $(AuPPh_3)_2A_2T_3$. Removing these constraints in [*n*-$Bu_4N]_2[(AuCN)_2A_2T_3$] still does not give aurophilic interactions, presumably because of intercalation of the cation between the Au centers. It is only in $Au_2(dppm)(A_2T_3)$, with the bridging dppm and no cations present, that an aurophilic interaction is observed. This reluctance to form aurophilic interactions suggests that these are weak here and observed only with forcing conditions. The conjugation in the terthiophene backbone is also found to depend on steric influences. In the solid state, the greatest conjugation (as assessed by the interannular torsion angles and the visible absorption spectra) is found in $Au_2(dppm)(A_2T_3)$. Interestingly, this compound is the only one which does not emit at room temperature, an effect attributed to either the presence of a low-lying triplet state because of the highly conjugated terthiophene or to a deactivating pathway resulting from the aurophilic interaction.

Photoinduced electron transfer was explored by irradiation of the complexes in the presence of an electron acceptor, MV^{2+}. [*n*-$Bu_4N]_2[(AuCN)_2A_2T_3$] did not undergo PET to MV^{2+}, possibly because of the formation of an ion pair in which rapid back electron transfer can occur. $(AuPPh_3)_2A_2T_3$ and $Au_2(dppm)(A_2T_3)$ both undergo PET to MV^{2+} with UV light excitation, but only $(AuPPh_3)_2A_2T_3$ undergoes photoinduced electron transfer with MV^{2+} with broadband white light. These differences are attributed to electronic effects, possibly related to either the rigidity or aurophilic interaction of $Au_2(dppm)(A_2T_3)$, allowing PET in the case of $(AuPPh_3)_2A_2T_3$ but not for $Au_2(dppm)(A_2T_3)$.

All of the complexes exhibited a terthiophene-based oxidation wave in the CV, and $Au_2(dppm)(A_2T_3)$ also has a $Au^{+/2+}$ oxidation wave. All of the Au complexes electropolymerize, and the presence of the aurophilic interaction in $Au_2(dppm)(A_2T_3)$ does not inhibit electropolymerization; thus, this is the first example of a complex with an intramolecular Au−Au interaction which electropolymerizes.

Experimental Section

General Procedures. 3,3″-Dibromo-2,2′:5′,2″-terthiophene (Br_2T_3),[31] AuCl(tht)[69] (tht = tetrahydrothiophene), and methyl viologen hexafluorophosphate (MV^{2+})[70] were prepared according to slightly modified literature procedures. $Au(PPh_3)Cl$ was prepared by addition of triphenylphosphine to AuCl(tht).[71] [*n*-Bu_4N]CN, triphenylphosphine (PPh_3), bis(diphenylphosphino)methane (dppm), methyl viologen chloride and CuI were purchased from Sigma-Aldrich, $HAuCl_4$ and $Pd(PPh_3)_4$ were purchased from Strem Chemicals, [*n*-Bu_4N][PF_6] was purchased from Fluka Chemicals, and trimethylsilylacetylene was purchased from Acros Chemicals.

^1H, $^{13}C\{^1H\}$, and $^{31}P\{^1H\}$ NMR spectra were collected on either a Bruker AV-300 spectrometer or a Bruker AV-400 spectrometer. ^1H and $^{13}C\{^1H\}$ NMR spectra were referenced to residual solvent, and $^{31}P\{^1H\}$ NMR spectra referenced to external 85% H_3PO_4. Infrared spectra were obtained on a Nicolet 6700 FTIR with a Smart Orbit accessory. Solution and solid-state UV−vis absorption spectra were obtained on a Varian Cary 5000 UV−vis−near-IR spectrophotometer. Solution excitation and emission spectra were obtained on a Photon Technology International QuantaMaster fluorimeter and were uncorrected for lamp intensity. Low temperature absorption and emission spectra were obtained from 4:1 ethanol/methanol solutions using an Oxford OptistatDN cryostat. The limited solubility of $(AuPPh_3)_2A_2T_3$, $Au_2(dppm)(A_2T_3)$, and A_2T_3 in the alcohol mixture required dissolving them in a small amount of DMF prior to addition to the ethanol/methanol. Quantum yields were measured using a Labsphere general purpose integrating sphere.

(69) Uson, R.; Laguna, A.; Vicente, J. *J. Organomet. Chem.* **1977**, *131*, 471–475.
(70) Manjula, A.; Nagarajan, M. *ARKIVOC* **2001**, 165–183.
(71) Gunatilleke, S. S.; Barrios, A. M. *J. Med. Chem.* **2006**, *49*, 3933–3937.

Fluorescence lifetime measurements were carried out on a Princeton Instruments Spectra Pro 2300i Imaging Triple Grating Monochromator/Spectrograph with a Hamamatsu Dynamic Range Streak Camera (excitation source: EKSPLA Nd:YAG laser, $\lambda = 355$ nm). Samples were prepared with an optical density of 0.1 at the maximum of the lowest energy absorption band. Cyclic voltammetry was carried out using an Autolab potentiostat. Either a platinum disk or indium tin oxide (ITO) on a glass slide was used as the working electrode. The reference electrode was a silver wire, and the counterelectrode was platinum mesh. Decamethylferrocene was used as an internal reference to correct the potentials to the saturated calomel electrode (SCE). The electrolyte, [*n*-Bu_4N][PF_6], was recrystallized three times from ethanol and heated to 90 °C under vacuum for 3 days prior to use. Cyclic voltammetry was carried out in CH_2Cl_2 dried over an activated alumina column. Solutions contained 0.1 M [*n*-Bu_4N][PF_6] and 1×10^{-3} M of the appropriate compound. EI mass spectra were obtained using a Kratos MS-50 double focusing mass spectrometer coupled to a MASPEC data system. The samples were introduced using direct insertion probe. ESI mass spectra were recorded on Bruker Esquire-LC ion trap mass spectrometer equipped with an electrospray ion source. The solvent for the ESI-MS experiments was methanol, and the concentration of the compound was ~10 μM. MALDI mass spectra were obtained on a Bruker Biflex IV MALDI-TOF instrument equipped with a nitrogen laser. The samples were dissolved in methanol or chloroform, and the MALDI mass spectra acquired in positive reflectron mode with delay extraction. Spectra were obtained by averaging 100 laser shots. Calibration of the MALDI-TOF spectra was performed externally using peptide standards. The CHN elemental analysis was performed using an EA1108 elemental analyzer, using calibration factors. The calibration factor was determined by analyzing a suitable certified organic standard (OAS) of a known elemental composition. X-ray photoelectron spectroscopy (XPS) analysis was performed using a Leybold MAX200 spectrometer equipped with an Al Kα source with a pass energy of 192 eV and the sampling area was 2 × 4 mm.

Synthesis. ***Caution!*** *Although no explosions were encountered here, Au acetylide complexes have previously been shown to be explosive*[64,72,73] *and care must be exercised when working with them.*

3,3″-Di(trimethylsilylethynyl)-2,2′:5′,2″-terthiophene. A degassed piperidine solution (50 mL) of Br_2T_3 (1.160 g, 2.86 mmol), trimethylsilylacetylene (10.1 g, 102.8 mmol), $Pd(PPh_3)_4$ (330 mg, 0.29 mmol) and CuI (59.8 mg, 0.314 mmol) was heated to reflux in the dark for 5 days. After cooling the reaction to room temperature, 50 mL of Et_2O was added, and the mixture was washed five times with 50 mL of H_2O. The Et_2O was then removed in vacuo leaving a brown oil. The oil was partially purified via column chromotography on silica with hexanes as the eluent. The resulting red oil (1.18 g) contained some trimethylsilyl impurities which were difficult to remove, and the compound was used without further purification in the subsequent reaction. When a sample of the oil was left dissolved in hexanes at −4 °C for 3 months, pure yellow 3,3″-di(trimethylsilylethynyl)-2,2′:5′,2″-terthiophene precipitated from the solution. ^{1}H NMR (300 MHz, $CDCl_3$); δ 7.61 (s, 2H), 7.08 (d, 2H, $J = 5.1$ Hz), 7.06 (d, 2H, $J = 5.4$ Hz), 0.31 (s, 18H). $^{13}C\{^1H\}$ NMR (75 MHz, $CDCl_3$); δ 135.7, 131.7, 125.9, 117.7, 100.7, −0.14, (no resonances attributed to the acetylenic carbons were observed). EI-MS *m*/*z* 440 (100%, $[M]^+$). Anal. Calcd for $C_{22}H_{24}Si_2S_3$: C, 59.95; H, 5.49. Found: C, 59.66; H, 5.73.

3,3″-Diethynyl-2,2′:5′,2″-terthiophene (A_2T_3). A THF solution of *n*-Bu_4NF (1 M, 5.9 mL) was added to a stirring THF solution (50 mL) of 3,3″-di(trimethylsilylethynyl)-2,2′:5′,2″-terthiophene (1.18 g, 2.68 mmol). The solution immediately changed from yellow to dark brown and was stirred overnight. The THF was then removed in vacuo, and the subsequent residue was dry loaded on a silica column and purified with an acetone/hexanes (1:2) eluent. A_2T_3 was collected as a yellow solid. Yield: 512 mg (65%). Crystals suitable for X-ray diffraction were grown from CH_2Cl_2/hexanes solution. ^{1}H NMR (300 MHz, $CDCl_3$); δ 7.51 (2, 2H), 7.11 (q, 4H, $J = 5.1$ Hz), 3.43 (s, 2H). $^{13}C\{^1H\}$ NMR (100 MHz, $CDCl_3$) δ 140, 136, 132, 126, 123, 117, 82, 79. IR 2100 cm^{-1} (ν(C≡C)). EI-MS *m*/*z* 296 (100%, $[M]^+$). Anal. Calcd for $C_{16}H_8S_3$: C, 64.83; H, 2.72. Found: C, 64.54; H, 2.75.

($AuPPh_3$)$_2A_2T_3$. To a stirred $CHCl_3$ solution (50 mL) of $AuCl(PPh_3)$ (245 mg, 0.495 mmol) and A_2T_3 (73 mg, 0.247 mmol), NEt_3 (3 mL) was added. The solution was left stirring at room temperature for 48 h. The $CHCl_3$ was then removed in vacuo, and the residue was washed several times with 5 mL aliquots of water. The residue was washed with acetone and subsequently dissolved in minimal $CHCl_3$ and hexanes was added. The solution was cooled to 4 °C, and a yellow crystalline precipitate formed. The precipitate was vacuum filtered to obtain 267 mg (0.220 mmol, 89% yield) of $(AuPPh_3)_2A_2T_3$. Crystals suitable for X-ray diffraction were grown from $CHCl_3$/hexanes solution. ^{1}H NMR (400 MHz, $CDCl_3$): δ 7.67 (s, 2H), 7.56 (m, 10H), 7.40 (m, 20H), 7.02 (d, 2H, $J = 5.1$ Hz), 6.98 (d, 2H, $J = 5.1$ Hz). $^{31}P\{^1H\}$ NMR (121 MHz, $CDCl_3$): δ 42.05. MALDI-TOF-MS *m*/*z* 1212 ($[M]^+$). Anal. Calcd for $C_{52}H_{36}Au_2P_2S_3 \cdot CHCl_3$: C, 47.78; H, 2.79. Found: C, 47.93; H, 2.89. IR 2226 cm^{-1} (ν(C≡C)).

[*n*-Bu_4N]$_2$[($AuCN$)$_2A_2T_3$]. A CH_2Cl_2 solution (10 mL) containing $(AuPPh_3)_2A_2T_3$ (100 mg, 0.0824 mmol) and *n*-Bu_4NCN (46.4 mg, 0.173 mmol) was sonicated at room temperature for 9 min. Immediately, hexanes (20 mL) were added, and the solution sonicated for another 9 min during which time a precipitate formed. The mixture was left undisturbed for 1 h, and then the hexanes/CH_2Cl_2 solution was decanted from the solid residue. The residue was rinsed twice with hexanes (5 mL), then dissolved in 5 mL of a 1:1 mixture of acetone and diethyl ether. The acetone/ether solution was left at 4 °C overnight, during which time bright yellow crystals of [*n*-$Bu_4N]_2[(AuCN)_2A_2T_3$] formed and were collected by vacuum filtration (60 mg, 0.049 mmol, 59%). The crystals were suitable for X-ray diffraction. ^{1}H NMR (400 MHz, $CDCl_3$): δ 7.95 (s, 2H), 7.00 (s, 4H), 3.18 (t, 16 H, $J = 8.4$ Hz), 1.64 (m, 16 H), 1.43 (m, 16 H), 0.99 (m, 24 H). Negative ESI-MS *m*/*z* 982 (100%, [M-*n*-$Bu_4N]^-$). Anal. Calcd for $C_{50}H_{78}Au_2N_4S_3$: C, 49.01; H, 6.42; N, 4.57. Found: C, 49.41; H, 6.43; N, 4.91. IR 2138 cm^{-1} (ν(C≡N)); 2105 cm^{-1} (ν(C≡C)).

Au_2(dppm)(A_2T_3). A CH_2Cl_2 (20 mL) solution of $(AuPPh_3)_2A_2T_3$ (121 mg, 0.0998 mmol) and dppm (38 mg, 0.0998 mmol) was sonicated at room temperature for 30 min. Immediately, hexanes (20 mL) were added to the solution and sonicated for 9 min during which time a solid precipitate formed. The solid was washed twice with hexanes (20 mL), and the residue dissolved in 5 mL of a 1:0.25:1 $CHCl_3/CH_2Cl_2$/acetone solution and left to crystallize. Dark orange crystals of $Au_2(dppm)(A_2T_3)$ formed overnight and were washed three times with acetone. Yield: 51 mg (48%). Crystals suitable for single crystal X-ray diffraction were grown from a $CHCl_3/CH_2Cl_2$/acetone solution. ^{1}H NMR (300 MHz, $CDCl_3$): δ 7.65 (m, 8H), 7.44 (m, 4H), 7.35 (m, 8H), 7.19 (s, 2H), 7.08 (d, 2H, $J_{HH} = 5.4$ Hz), 7.00 (d, 2H, $J_{HH} = 5.4$ Hz), 3.68 (t, 2H, $J_{PH} = 10.7$ Hz). $^{31}P\{^1H\}$ NMR (121 MHz, $CDCl_3$): δ 32.3 (s). TOF *m*/*z* 1073 ($[M]^+$). Anal. Calcd for $C_{41}H_{28}Au_2P_2S_3 \cdot (CH_3)_2CO$: C, 46.73; H, 3.03. Found: C, 46.64; H, 3.12. IR 2107 cm^{-1} (ν(C≡C)).

X-ray Crystallography. All crystals were mounted on glass fibers. All measurements were made on a Bruker X8 APEX II diffractometer with graphite monochromated Mo−Kα radiation. Data were collected and integrated using the Bruker

(72) Mathews, J. A.; Watters, L. L. *J. Am. Chem. Soc.* **1900**, *22*, 108–111.
(73) McArdle, C. P.; Jennings, M. C.; Vittal, J. J.; Puddephatt, R. J. *Chem.—Eur. J.* **2001**, *7*, 3572–3583.

SAINT[74] software package. Data were corrected for absorption effects using the multiscan technique (SADABS[75]). The data were corrected for Lorentz and polarization effects. The structures were solved by direct methods.[76]

A_2T_3. All data were collected to a maximum 2θ value of 55.0°. Data were collected in a series of ϕ and ω scans in 0.50° oscillations with 10.0 s exposures. The crystal-to-detector distance was 36.00 mm. Of the 18307 reflections that were collected, 3066 were unique (R_{int} = 0.040); equivalent reflections were merged. The linear absorption coefficient, μ, for Mo−Kα radiation is 5.16 cm^{-1}. The minimum and maximum transmission coefficients were 0.812 and 0.975, respectively. All non-hydrogen atoms were refined anisotropically. All hydrogen atoms were placed in calculated positions but were not refined. The final cycle of full-matrix least-squares refinement on F^2 was based on 3066 reflections and 172 variable parameters and converged.

$(AuPPh_3)_2A_2T_3$. Data were collected in a series of ϕ and ω scans in 0.50° oscillations with 20.0 s exposures. The crystal-to-detector distance was 36.00 mm. The data were collected to a maximum 2θ value of 56.0°. Of the 32338 reflections that were collected, 5733 were unique (R_{int} = 0.034); equivalent reflections were merged. The linear absorption coefficient, μ, for Mo−Kα radiation is 64.02 cm^{-1}. Data were corrected for absorption effects using the multiscan technique (SADABS),[75] with minimum and maximum transmission coefficients of 0.530 and 0.726, respectively. The material crystallizes with one-half-molecule in the asymmetric unit, residing on a 2-fold axis of rotation. All non-hydrogen atoms were refined anisotropically. All hydrogen atoms were placed in calculated positions but were not refined. There was unresolvable solvent ($CHCl_3$, CH_2Cl_2 or hexanes) in the lattice. As a result the PLATON/SQUEEZE[77] program was used to generate a "solvent-free" data set. The final cycle of full-matrix least-squares refinement on F^2 was based on 5733 reflections and 267 variable parameters and converged (largest parameter shift was 0.00 times its esd).

[*n*-$Bu_4N]_2[(AuCN)_2A_2T_3]$. The data were collected to a maximum 2θ value of 56.2°. Data were collected in a series of ϕ and ω scans in 0.50° oscillations with 10.0 s exposures. The crystal-to-detector distance was 36.00 mm. Of the 61962 reflections that were collected, 12644 were unique (R_{int} = 0.055); equivalent reflections were merged. The linear absorption coefficient, μ, for Mo−Kα radiation is 64.02 cm^{-1}. Data were corrected for absorption effects using the multiscan technique (SADABS),[75] with minimum and maximum transmission coefficients of 0.204 and 0.501, respectively. All non-hydrogen atoms were refined anisotropically. All hydrogen atoms were placed in calculated positions but were not refined. The material crystallizes with a small amount of disorder in one thiophene along with its C−C−Au−C−N substituent. The minor disordered fragment was refined using geometric restraints, as well as restraints on anisotropic displacement parameters. The final cycle of full-matrix least-squares refinement on F^2 was based on 12644 reflections and 571 variable parameters.

Au_2(dppm)(A_2T_3). The data were collected to a maximum 2θ value of 56.2°. Data were collected in a series of ϕ and ω scans in 0.50° oscillations with 5.0 s exposures. The crystal-to-detector distance was 40.00 mm. Of the 57624 reflections that were collected, 9505 were unique (R_{int} = 0.053); equivalent reflections were merged. The linear absorption coefficient, μ, for Mo−Kα radiation is 77.64 cm^{-1}. The minimum and maximum transmission coefficients were 0.190 and 0.537, respectively. All non-hydrogen atoms were refined anisotropically. All C−H hydrogen atoms were placed in calculated positions but were not refined. The final cycle of full-matrix least-squares refinement on F^2 was based on 9505 reflections and 469 variable parameters and converged (largest parameter shift was 0.00 times its esd) with unweighted and weighted agreement factors.

Photoinduced Electron Transfer to MV^{2+}. A solution of 4×10^{-3} M of either methyl viologen chloride or methyl viologen hexafluorophosphate was degassed via three freeze−pump−thaw cycles. Solutions (10^{-5} M) of the respective Au complexes and A_2T_3 were prepared and degassed. Approximately 1.5 mL of the methyl viologen solution and 1.5 mL of the acetylide compound solution were added to a cuvette under N_2(g). An absorption spectrum was collected to ensure no decomposition of any reactants occurred. This solution was then irradiated with a hand-held lamp (λ_{max} = 365 nm, intensity ~0.5 mW) or a white lamp (400−800 nm broadband light, intensity ~50 mW) for 15−16 min. Lamp intensity powers were measured with an Ophir power meter thermal sensor. After irradiation, the absorption spectrum of the solution was collected again.

Acknowledgment. We thank the Natural Sciences and Engineering Research Council of Canada for funding, the Laboratory for Advanced Spectroscopy and Imaging Research (LASIR) for access to spectroscopic equipment, Dr. Saeid Kamal for assistance with the lifetime measurements, and Dr. Ken Wong for XPS data. A.M.K. thanks UBC and Mountain Equipment Coop (MEC) for graduate fellowships.

Supporting Information Available: X-ray crystallographic data for A_2T_3, $(AuPPh_3)_2A_2T_3$, [*n*-$Bu_4N]_2[(AuCN)_2A_2T_3]$, and Au_2(dppm)(A_2T_3) in CIF format. Spectra of irradiated solutions of complexes and MV^{2+}, cyclic voltammogram of A_2T_3. This material is available free of charge via the Internet at http://pubs.acs.org.

(74) *SAINT*, Version 7.53A; Bruker AXS Inc.: Madison, WI, 1997−2008.
(75) *SADABS, Bruker Nonius area detector scaling and absorption correction*, V2008/1; Bruker AXS Inc.: Madison WI, 2008.
(76) Altomare, A.; Burla, M. C.; Camalli, M.; Cascarano, G. L.; Giacovazzo, C.; Guagliardi, A.; Moliterni, A. G. G.; Polidori, G.; Spagna, R. *J. Appl. Crystallogr.* **1999**, *32*, 115–119.
(77) Sluis, P. v. d.; Spek, A. L. *Acta Crystallogr., Sect. A* **1990**, *46*, 194–201.